Acta Geotechnica (2025) 20:185–196
https://doi.org/10.1007/s11440-024-02433-6

RESEARCH PAPER

Constitutive behaviour of a granular matrix containing coal mine waste intermixed with rubber crumbs

A. S. M. Riyad[1] · Buddhima Indraratna[1] · Yujie Qi[2] · Miriam Tawk[3]

Received: 19 February 2024 / Accepted: 9 October 2024 / Published online: 1 November 2024

Abstract

Traditional railway substructure materials (i.e., natural crushed rock aggregates used for ballast and capping layers) degrade under service loads, incurring higher periodic maintenance costs compared to recycled materials. Using recycled waste materials such as coal wash and rubber crumbs for infrastructure upgrades not only reduces construction and maintenance costs but also supports environmental sustainability. By exploring unconventional avenues, earlier studies have delved into the viability of blending rubber crumbs (RC) and coal wash (CW) as an innovative substitute for traditional railway substructure materials, with a specific focus on the capping layer. This study introduces a semi-empirical constitutive model to simulate the response of mixtures of coal wash and rubber crumbs (CWRC) using the bounding surface plasticity framework. The novelty of this study is that a modified volumetric strain expression is introduced to capture the compressibility of rubber, thus enabling a more accurate representation of the internal deformation of rubber within the granular matrix. The variation of rubber content in the mixture is captured by the corresponding critical state void ratio surface and the hardening modulus. The theoretical model is then calibrated and validated using static drained triaxial test data for CWRC mixtures as well as mixtures of steel furnace slag, coal wash, and rubber crumbs (SFS + CW + RC).

Keywords Bounding surface plasticity · Coal wash (CW) · Constitutive model · Modified volumetric strain · Rubber crumbs (RC)

1 Introduction

Coal wash (CW) is the residual granular material that is generated during a process known in the coal mining industry as "washing" [20]. Rubber crumbs (RC) are produced from discarded tires which are shredded and then ground to produce smaller particles [24]. These waste products cannot be used independently to replace traditional granular materials because of their undesirable geotechnical properties such as the excessive deformation of rubber and particle degradation of CW [10, 13, 19, 25]. To overcome their individual adverse properties, CW and RC can be mixed together or with other materials and then used in civil engineering projects. Rubber is often favoured as a secondary material in blends because of its lightweight and energy-absorbing properties. CW could also be blended with fly ash, soil, concrete, conventional aggregates, and slag for use in transportation infrastructure projects [5, 8, 11, 18, 36, 39]. To minimize the degradation of CW

✉ Buddhima Indraratna
buddhima.indraratna@uts.edu.au

A. S. M. Riyad
a.s.riyad@student.uts.edu.au

Yujie Qi
yujie.qi@uts.edu.au

Miriam Tawk
miriam.tawk@lau.edu.lb

[1] Transport Research Centre, Faculty of Engineering & Information Technology, School of Civil and Environmental Engineering, University of Technology Sydney (UTS), Sydney, NSW 2007, Australia

[2] Faculty of Engineering & Information Technology, School of Civil and Environmental Engineering, University of Technology Sydney (UTS), Sydney, NSW 2007, Australia

[3] Department of Civil Engineering, Lebanese American University, Byblos 1102 2801, Lebanon

and encourage its uses in applications where a dynamic loading is applied (i.e., railway capping layer), RC can be introduced into the granular matrix to enhance its energy absorption properties as described by Indraratna et al. [14].

Indraratna et al. [14], Hunt et al. [12], and Tawk and Indraratna [37], explored the geotechnical characteristics of CWRC mixtures under static loading conditions and found that adding rubber can minimize particle breakage of CW particles. However, a mathematical approach can provide a more in-depth understanding of the influence of RC on the geotechnical properties of these waste granular mixes. While numerous laboratory studies on the behaviour of soil-rubber or waste-rubber mixtures were undertaken, only a few studies concentrated on the theoretical models within a constitutive framework.

Several constitutive models have been reported in the literature for rubber-aggregate mixtures [19, 21, 22, 24, 37, 41]. Lee et al. [19] adopted Duncan et al. [7]'s hyperbolic model to capture the monotonic behaviour of sand-rubber mixtures. However, this model failed to capture the post-peak strain softening behaviour, plastic strains, and the dilative response of rubber-aggregate mixtures. Mashiri et al. [21] and Youwai and Bergado [41] used a hypo-plasticity model to simulate the static behaviour of sand-shred tire/tire chip blends. However, since the behaviour of rubber crumbs mixed with rigid aggregates is different from that of tire shreds or chips [4], their model may not adequately represent the behaviour of waste materials-rubber crumbs combinations. In this regard, Qi et al. [24] developed a semi-empirical elasto-plastic constitutive model based on the bounding surface concept. Although the influence of rubber content was generally captured in this model, the specific effect of the internal deformation of rubber crumbs (compressibility) on the behaviour of the blended mixture was not investigated. Tawk and Indraratna [37] developed a model within a critical state (CS) framework to consider the effect of compressible components such as rubber on the monotonic behaviour of coal wash-rubber crumbs (CWRC) mixtures; they proposed a modified void ratio to account for the compressibility of rubber particles within the mixture. While the effect of rubber inclusion on the volumetric deformation of the mixture was considered in their model, they did not assess the effect of hardening on the stress–strain relationship.

In view of the above, the current study presents a constitutive model for CWRC mixtures under static loading conditions by adopting the Nor-Sand model [17]. Nor-Sand constitutes a basic elastoplastic model delineated by a bounding surface, featuring a hardening law intricately linked to the critical state theory by incorporating the state parameter index [15]. The benefits of utilizing the bounding surface plasticity theory, as opposed to conventional elastic-plasticity theory, lie in the incorporation of a flexible formulation for the loading surface and the bounding surface. This feature serves to eliminate the abrupt transition from elastic to elastic–plastic behaviour [31], thus enabling the current to simulate more accurately the stress dilatancy and strain-softening behaviour of densely compacted materials. Moreover, the current study utilizes a modified volumetric expression, inspired by Tawk and Indraratna [37], to capture the compressibility of rubber, resulting in a more accurate portrayal of its internal deformation within the granular matrix. Therefore, the critical state void ratio and the hardening modulus are dependent upon the content of rubber crumbs in the mixture. The experimental findings from a series of consolidated drained triaxial tests on saturated CWRC mixtures (with a rubber content $X_{RC} = 0$ to 15% of rubber by mass) at three confining pressures (25, 50, and 75 kPa), as reported by Indraratna et al. [14], are used to calibrate and validate the proposed constitutive model. Here, X_{RC} is the ratio of the mass of RC and the mass of CW. In addition, completely independent data sets obtained from a previous study on SFS + CW + RC mixtures [26] are also used to validate the proposed model. Figure 1 shows the particle size distribution of coal mine waste and rubber crumbs for the two cases examined. In CWRC mixtures, the mean particle size of coal wash $\left(D_{50,cw}\right)$ is 1.8 times that of the rubber crumbs $\left(D_{50,RC}\right)$, whereas in SFS + CW + RC mixtures, this ratio ranges from 0.8 to 2.3.

2 Effect of rubber on the void ratio and critical state

Rubber exhibits characteristics of a viscous elastic material, with a typical Poisson's ratio (μ) close to 0.5 under normal conditions, indicating insignificant volumetric

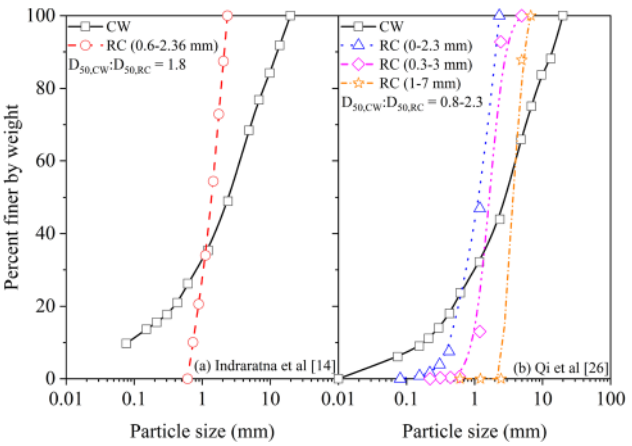

Fig. 1 Particle size distribution of CW and RC

strain. However, under increased confining pressure, the Poisson's ratio tends to decrease, allowing for some volumetric deformation to occur in rubber particles. While proctor compaction tests do not subject rubber to prolonged axial pressure or at levels significant enough to induce substantial compression, the confining pressure and axial stress applied in triaxial tests can compress rubber particles, resulting in noticeable volumetric deformation. Consequently, it is expected that the maximum compressive volumetric strain will increase with higher rubber content, partly due to the deformation of the rubber particles themselves. Therefore, the void ratio equation commonly used for incompressible rigid aggregates is not applicable when incorporating compressible components like rubber within the matrix of pure granular materials tested under triaxial conditions. Therefore, the modified void ratio (e^*) for rubber-mixed granular material is adopted in this research [37], and it is expressed as:

$$e^* = e_0^* + \varepsilon_v^*(1 + \omega_0) \tag{1}$$

where e_0^* is the initial modified void ratio before the mixture is sheared, ε_v^* is the void volumetric strain associated with the change in the volume of voids only, and ω_0 is the initial compressibility ratio. When the solid phase in the mixture is assumed to be incompressible, the total volumetric strain ε_v is equal to the void volumetric strain ε_v^*. Tawk and Indraratna [37] reported that classical soil mechanics principles (e.g. weight-volume relations) could not be directly applied to granular mixtures containing compressible rubber crumbs. In this context, the rubber content can be considered to represent an equivalent (modified) void space with distinct physical characteristics within the granular mixture. For instance, altering the initial rubber content then contributes to a change in the initial relative density, hence a corresponding change in the equivalent or modified initial void ratio. In other words, the classical equation for the initial void ratio is modified to capture the influence of compressible rubber crumbs. The initial modified void ratio is calculated as (Appendix B):

$$e_0^* = e_0\left(1 + \frac{X_{\mathrm{RC}}}{100} \times \frac{G_{\mathrm{s,CW}}}{G_{\mathrm{s,RC}}}\right) \tag{2}$$

where e_0 and X_{RC} are the initial void ratio and the percentage of rubber crumbs, respectively, and $G_{\mathrm{s,CW}}$ and $G_{\mathrm{s,RC}}$ are the values of the specific gravity of coal wash and rubber crumbs, respectively. The compressibility ratio is expressed as:

$$\omega_0 = e_0^* + \frac{X_{\mathrm{RC}}}{100} \times \frac{G_{\mathrm{s,CW}}}{G_{\mathrm{s,RC}}} \tag{3}$$

The void volumetric strain, accounting for the compressibility of rubber crumbs and the initial modified void ratio before the mixture is sheared, is then derived as:

$$\varepsilon_v^* = \frac{e^* - e_0^*}{1 + \omega_0} \tag{4}$$

The critical state (CS) is where a soil sample experiences ignorable changes in volume and deviator stress with increasing axial strain. It is noted that the CS for CWRC mixtures is hard to achieve under current triaxial test conditions due to the limitation of the maximum axial strain that can be achieved (i.e. 25%); a similar observation was reported for rubber-sand mixtures [22] and for SFS + CW + RC mixtures [26]. Thus, the CS parameters listed in Table 1 were obtained by Tawk and Indraratna [37] by extrapolating the stress–strain curve and the axial strain-volumetric strain curves. Moreover, a constant critical state stress ratio M_{cs} was identified for all the tested CWRC mixtures, while the critical state void ratio kept changing with varying rubber contents. Figure 2a shows a linear critical state void ratio line (CSVL) in the $e^* - lnp\prime$ plane for all CWRC mixtures. The CSVL can be expressed as:

$$e_{\mathrm{cs}} = \Gamma - \lambda lnp' \tag{5}$$

where Γ and λ represent the modified void ratio at $p' = 1$ kPa and the gradient of the CSVL, respectively. It is evident from Fig. 2a that the CSVL of these granular mixtures containing rubber is not unique, and it rotates in a clockwise direction as the percentage of rubber increases. This can be attributed to the compressibility and deformability of rubber particles, which can result in a reduction in the effective stress transmitted between particles, leading to decreased strength and stiffness of the granular matrix.

Table 1 Model parameters for CWRC mixtures and SFS + CW + RC mixtures

Data source	Indraratna et al. [14]	Qi et al. [26]
μ	$0.4 - 0.016X_{\mathrm{RC}}$	$0.3 + 0.002X_{\mathrm{RC}}$
Γ	$0.46 + 0.013X_{\mathrm{RC}}$	$0.64 + 0.01X_{\mathrm{RC}}$
λ	$0.026 + 0.0014X_{\mathrm{RC}}$	$0.069 + 0.003X_{\mathrm{RC}}$
κ	$0.01\exp(0.19X_{\mathrm{RC}})$	$0.002\exp(0.028X_{\mathrm{RC}})$
M_{cs}	1.54	$1.93 + 0.006X_{\mathrm{RC}}$
H_{min}	288.4	464.5
δ_H	0.07	0.016
β	0.13	0.63
N	$0.12\exp(0.06X_{\mathrm{RC}})$	$0.11\exp(0.02X_{RC})$
χ	$13.2 - 0.45X_{\mathrm{RC}}$	$14.0 - 0.16X_{RC}$
e_0	0.29	$0.466 + 0.0046\exp\left(\frac{X_{\mathrm{RC}}}{20.3}\right)$
G_s	$G_{s,\mathrm{CW}}\exp(-0.008X_{\mathrm{RC}})$	$G_{s,\mathrm{SFS+CW}}\exp(-0.0125X_{\mathrm{RC}})$

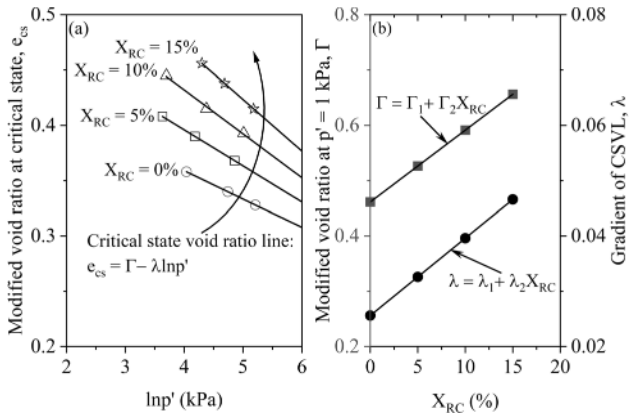

Fig. 2 **a** CSVL in the $e^* - lnp\prime$ plane and **b** CSV parameters (Modified after Tawk and Indraratna [37])

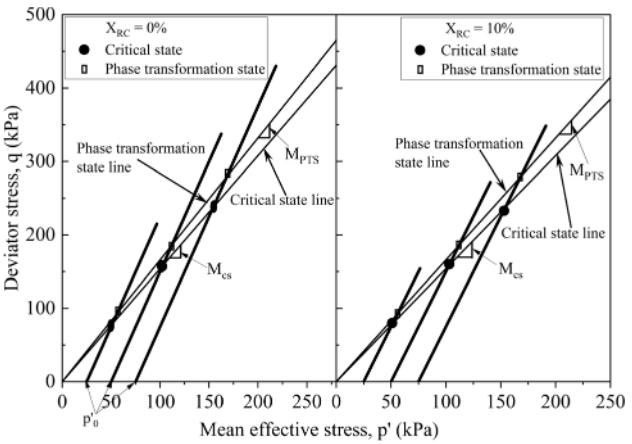

Fig. 4 CSL and PTS line in the $q - p\prime$ plane

This reduction in strength has the effect of causing the CSVL to rotate clockwise as the rubber content increases, indicating a transition toward a looser and more deformable state. Earlier research conducted by Tawk and Indraratna [37] and Qi et al. [26] for rubber-waste mixtures found that Γ and λ are linearly correlated with X_{RC} (Fig. 2b).

$$\Gamma = \Gamma_1 + \Gamma_2 X_{RC} \tag{6}$$

$$\lambda = \lambda_1 + \lambda_2 X_{RC} \tag{7}$$

The regression indices Γ_1, Γ_2, λ_1 and λ_2 are calculated based on the laboratory test data of CWRC mixture where X_{RC} ranges from 0 to 15%, as shown in Fig. 2b. The values of these parameters are shown in Table 1.

Substituting Eqs. (6) and (7) into Eq. (5), the critical state void ratio (CSV) surface shown in Fig. 3 is generated and is expressed as:

$$e_{cs} = (\Gamma_1 + \Gamma_2 X_{RC}) - (\lambda_1 + \lambda_2 X_{RC}) lnp' \tag{8}$$

Figure 4 illustrates the typical stress paths observed in monotonic triaxial tests in the $q - p\prime$ plane for CWRC mixtures with X_{RC} values of 0% and 10%. The critical state line (CSL), the phase transformation state (PTS) line and their corresponding stress ratio defined in Eq. (9) are shown in Fig. 4.

$$M_{cs,PTS} = \frac{q_{cs,PTS}}{p_{cs,PTS}\prime} \tag{9}$$

The PTS is a state in which the rate of incremental plastic volumetric strain is zero ($d\varepsilon_v^p = 0$), and it serves as the point at which the disruption of particle interlocking is initiated and the material changes from contraction to dilation. The stress ratio-dilatancy curves for CWRC mixture with X_{RC} values of 0% and 10% are shown in Fig. 5. Unlike the CS, the phase transformation state does not exhibit a zero incremental deviator stress ($dq \neq 0$). Figure 5 also shows that the stress ratio at peak deviator stress η_{max} decreases as the rubber content, X_{RC}, increases. Also, the corresponding dilatancy at the peak deviator stress, D^p_{peak}, decreases (Fig. 6). It is noteworthy that all

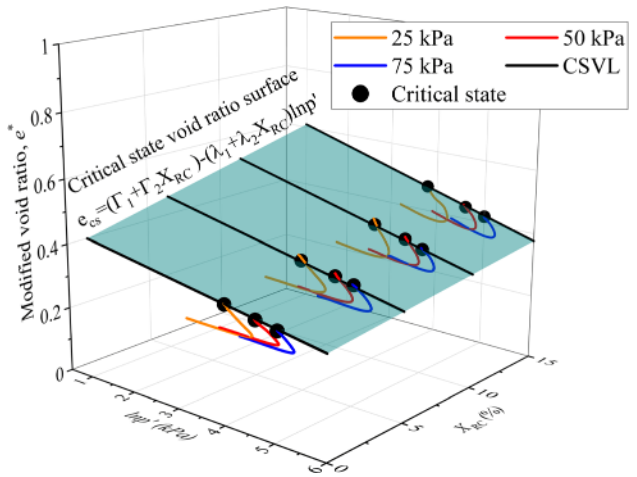

Fig. 3 CSV surface for CWRC mixtures in the $e^* - lnp' - X_{RC}$ space

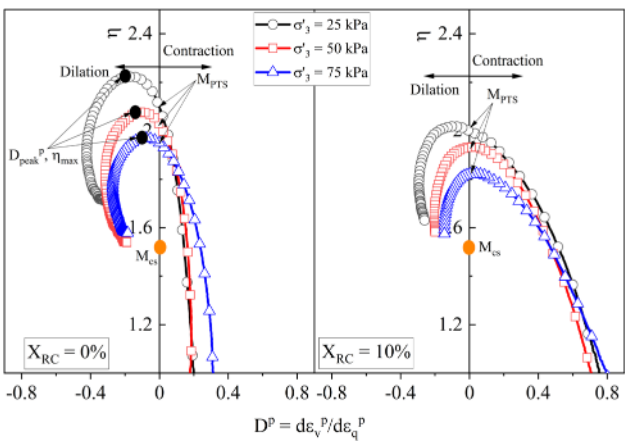

Fig. 5 Stress ratio-dilatancy curves for CWRC mixtures

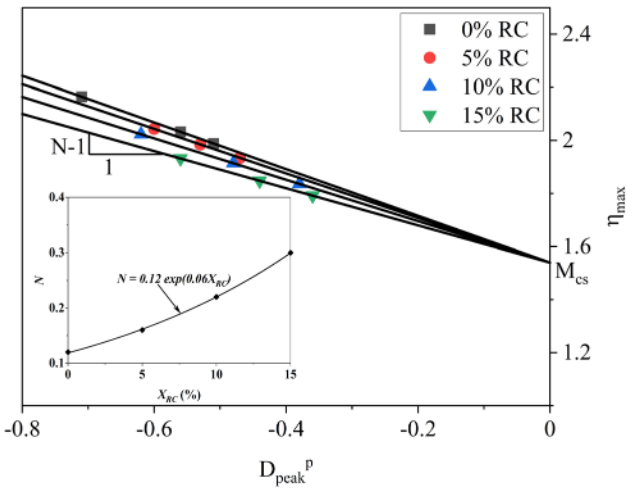

Fig. 6 Determination of M_{cs} and N

CWRC mixtures reach a constant $M_{\mathrm{cs}} = 1.54$. This implies that when dilation is initiated and the particles start to slide against each other, the overall frictional resistance decreases as the amount of X_{RC} increases, and the peak stress ratio $\eta_{\max}$ decreases. However, as the mixture approaches its CS and the number of contact points between particles is minimised, the impact on the stress ratio decreases. At this stage, the current stress ratio, after reaching its peak, is solely influenced by the frictional resistance of CW particles, especially when the amount of rubber is relatively low, specifically below 15% [37]. Furthermore, it is evident that CWRC mixtures prepared with a relatively dense state have a PTS ratio greater than the CS ratio, which is consistent with the trend observed by Youwai and Bergado [41] in sand-rubber mixtures with less than 40% of rubber.

The shear strength that develops during static triaxial testing is highly relevant to the strength at CS (intergranular friction) and interlocking between the grains (dilatancy). This could be established from the pioneering work of Taylor [38], and further demonstrated and uniquely described by Roscoe et al. [30]. Inspired by this concept, Roscoe and Schofield [28] defined the theory of stress-dilatancy developed by Taylor [38] using stress invariants. Nevertheless, it was eventually discovered that dilatancy or the degree of interlocking, did not play a significant role as originally assumed [3, 33]. To lessen the effect of dilatancy on the shear strength, Nova and Wood [23], among others, proposed a volumetric coupling parameter N, expressed in Eq. (10) and illustrated in Fig. 6.

$$\eta = (N-1)D^p + M_{\mathrm{cs}} \tag{10}$$

where $(\eta = \frac{q}{p'})$ is the effective stress ratio with $q = \sigma_1\prime - \sigma_3\prime$ and $p\prime = (\sigma_1\prime + 2\sigma_3\prime)/3$ being the deviatoric stress and mean effective stress, respectively; M_{cs} is the CS stress ratio; and $D^p = \frac{d\varepsilon_v^p}{d\varepsilon_q^p}$ is the plastic dilatancy, with $d\varepsilon_v^p$ and $d\varepsilon_q^p$ being the plastic volumetric strain increment and the plastic deviatoric strain increment, respectively. The parameter N can be determined by the slope of $\eta_{\max} - D^p_{\mathrm{peak}}$ curve as Fig. 6 shows. With an increasing rubber content (X_{RC}) in the mixtures, the value of the parameter N increases mainly due to the high elasticity and compressibility of rubber particles.

3 Loading surface and bounding surface

The concept of a bounding surface that was initially developed by Dafalias and Popov [6] is adopted in this study because of its adaptability and capacity to mimic the stress–strain behaviour of various types of soil [24, 32, 35]. Inspired by Jefferies and Been [17], the current study considers a bullet-shaped bounding surface that encompasses the triaxial compression part. It is assumed that the shape of the bounding surface is the same as that of the loading, i.e., for the bounding surface, $F_b(\overline{p\prime}, \overline{q}, \overline{p_c\prime}) = 0$ and for the loading surface, $f_L(p\prime, q, p_c\prime) = 0$ under densely compacted conditions (Fig. 7). The bounding surface and the loading surface are then expressed as [17]:

$$F_b(\overline{p'}, \overline{q}, \overline{p'_c}) = \left\{ \overline{q} - (M_{\mathrm{cs}} + N\psi_i\chi_i)\overline{p'}\left[1 + \ln\left(\frac{R\overline{p'_c}}{\overline{p'}}\right)\right]\right\} = 0, \ \text{for} \psi_i < 0 \tag{11}$$

$$f_L(p', q, p'_c) = q - (M_{cs} + N\psi_i\chi_i)p'\left[1 + \ln\left(\frac{Rp'_c}{p'}\right)\right] = 0, \ \text{for } \psi_i < 0 \tag{12}$$

where p'_c and $\overline{p'_c}$ are the intercepts of the loading surface and the bounding surface with the q = 0 axis, respectively;

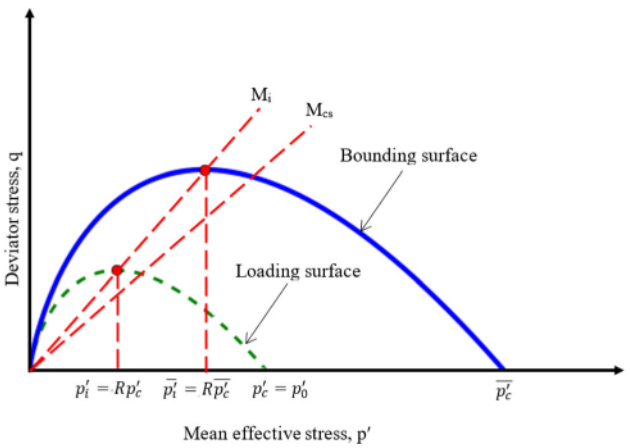

Fig. 7 Bounding surface and loading surface in the $q \sim p\prime$ plane

$(M_{cs} + N\psi_i\chi_i)$ is the stress ratio at the image state, presented as M_i in Fig. 7. The material constant R is used to express the ratio between $\overline{p_i\prime}$ and $\overline{p_c\prime}$ at the intercept of the bounding surface with the M_i line, which is also the same as the ratio between $p_i\prime$ and $p_c\prime$ at the intercept of the loading surface with the M_i line in the $q \sim p\prime$ plane; this determines the image stress point on the bounding surface and the loading surface, respectively. The coupling parameter N controls the size of loading surface. Figure 8 shows the variations in the size of the loading surface with the volumetric coupling parameter N. It is apparent that as N increases, the size of the loading surface and the strength of the material both increase when all other model parameters are constant.

Rearranging Eqs. (11) and (12) gives:

$$\frac{R\overline{p_c'}}{\overline{p'}} = \frac{Rp_c'}{p'} = \exp\left(\frac{\eta}{M_i} - 1\right) \tag{13}$$

In this approach, the evolution of the bounding surface is governed by the value of $\overline{p_c\prime}$, which has a strong correlation with the evolution of the volumetric strain, and the corresponding swelling line is depicted by:

$$e_{\kappa 0} - e^* - \kappa \ln p' = 0 \tag{14}$$

By intersecting the CSVL defined by Eq. (8) and the swelling line defined by Eq. (14) at the point $(e^*, \bar{p}\prime)$ and recalling Eq. (13), the position of the right point $\overline{p_c\prime}$ on the bounding surface can now be determined by:

$$\overline{p_c'} = \frac{p_r}{R}\exp\left(\frac{\Gamma - e^* - \kappa lnp'}{\lambda - \kappa}\right) \tag{15}$$

where p_r is a reference quantity with the dimensions of stress, necessary to establish dimensional consistency, and typically having the value of 1 kPa, λ and κ are the gradient of the CSVL and the swelling line in the $e^* - lnp\prime$ plane, respectively.

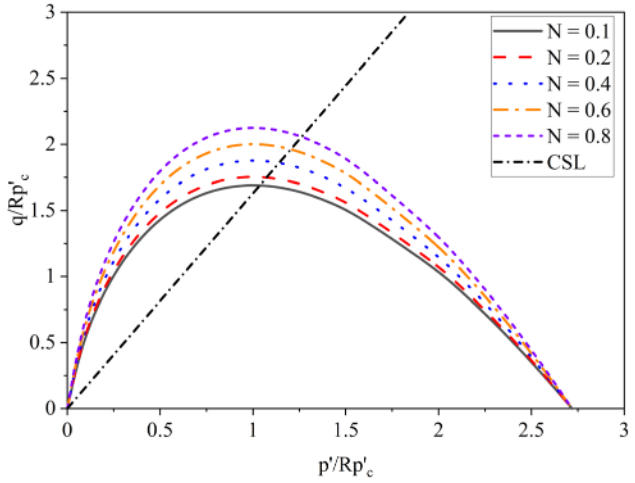

Fig. 8 Schematic presentation of the effect of different values of volumetric coupling parameter on the size of loading surface (CWRC mixture, $\sigma_3\prime = 25\text{kPa}, \text{RC} = 10\%$)

The unit normal loading vector $\hat{\boldsymbol{n}}$ at the image point defining the direction of loading is given using the general equation:

$$\hat{\boldsymbol{n}} = \frac{\partial f_L/\partial \sigma'}{\partial f_L/\partial \sigma'} = \frac{\partial F_b/\partial \overline{\sigma'}}{\partial F_b/\partial \overline{\sigma'}} = \begin{bmatrix} n_p \\ n_q \end{bmatrix} = \frac{1}{\sqrt{\left(\partial F_b/\partial \overline{p'}\right)^2 + \left(\partial F_b/\partial \overline{q}\right)^2}} \begin{bmatrix} \partial F_b/\partial \overline{p'} \\ \partial F_b/\partial \overline{q} \end{bmatrix} \tag{16}$$

Differentiating Eq. (11) with respect to $\overline{p'}$ and $\overline{q}$ gives:

$$\frac{\partial F_b}{\partial \bar{p}\prime} = -M_i \ln\left(\frac{R\overline{p_c\prime}}{\overline{p\prime}}\right) \tag{17}$$

$$\frac{\partial F_b}{\partial \overline{q}} = 1 \tag{18}$$

The components of $\hat{\boldsymbol{n}} = [n_p, n_q]^T$ at the effective stress on the bounding surface are defined as:

$$n_p = \frac{-M_i \ln\left(\frac{R\overline{p_c\prime}}{\overline{p\prime}}\right)}{\sqrt{\left\{-M_i \ln\left(\frac{R\overline{p_c\prime}}{\overline{p\prime}}\right)\right\}^2 + 1}} \tag{19}$$

$$n_q = \frac{1}{\sqrt{\left\{-M_i \ln\left(\frac{R\overline{p_c\prime}}{\overline{p\prime}}\right)\right\}^2 + 1}} \tag{20}$$

where $\overline{\sigma\prime}$ presents the effective stress on the bounding surface and $n_p$andn_q are components of the loading direction vectors.

4 Plastic flow rule

Roscoe [29] acknowledged the requirement of a strain invariant-based hardening law to relate with the CS due to the limitations of the original Cam-Clay model [28] and the modified Cam-Clay model [27] on the predicted behaviour of granular materials such as sand that could be established based on the stress-dilatancy theory. Therefore, Been and Jefferies [1] developed a state parameter for sands, and Jefferies [15] recommended using it as a strain invariant. Inspired by Wroth and Bassett [40], to capture and quantify the influence of unit weight and applied stress on the deformation of CWRC mixtures, the state parameter is expressed by:

$$\psi = e^* - e_{cs} \tag{21}$$

where ψ = state parameter; e^* = current modified void ratio; and e_{cs} = critical-state void ratio at the same mean effective stress.

However, the dilatancy at the peak deviator stress D^p_{peak} is linearly correlated with the state parameter at η_{max} $\left(\psi_{\eta_{\max}}\right)$ as shown in Fig. 9 and Eq. (22). As there is no elastic strain in the peak state, it can be stated that $D^p_{\text{peak}} = D_{\text{peak}}$, hence:

$$D_{\text{peak}} = D^p_{\text{peak}} = \chi\psi_{\eta_{\max}} \tag{22}$$

where χ is defined as the dilatancy constant. By considering the CS and capturing an image of it, denoted with the subscript i, the state parameter under the image state condition can be expressed by Eq. (23) [16]:

$$\psi_i = e^* - e_{\text{cs},\,i} = \psi + \lambda \ln\left(\frac{p_i}{p}\right) \tag{23}$$

In the above, the dilatancy constant at the image state condition is given by:

$$\chi_i = \frac{\chi M_{\text{cs}}}{M_{\text{cs}} - \lambda\chi} \tag{24}$$

where λ is the gradient of the CSVL in the $e^* - lnp'$ plane. At the bounding surface $\eta = \eta_{\max}$ and the image state ratio becomes:

$$M_{\text{i,max}} = M_{cs} + N * D^p_{\text{peak}} \tag{25}$$

Substituting Eqs. (10), (22) and (25) into Eq. (13) gives:

$$\left(\text{R}\overline{p'_c}\right)_{\max} = \overline{p'}\exp\left(\frac{-\psi_i\chi_i}{M_{\text{cs}} + N\psi_i\chi_i}\right) \tag{26}$$

The plastic dilatancy D^p, which is related to the plastic potential, can be obtained by substituting Eq. (10) into Eq. (11):

$$D^p = M_i \ln\left(\frac{\overline{p'}}{R\overline{p'_c}}\right) \tag{27}$$

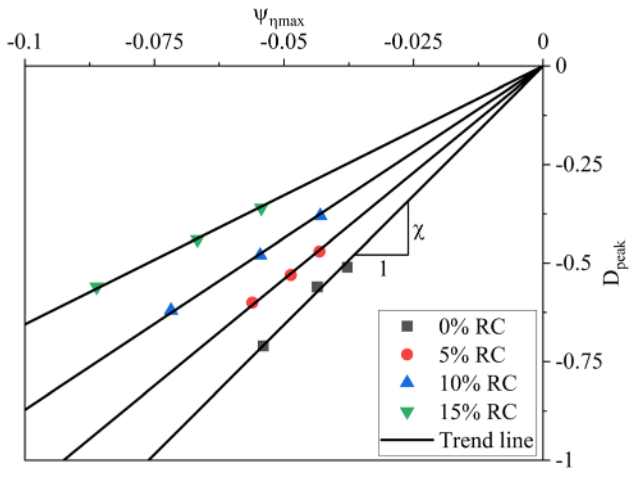

Fig. 9 Determination of dilatancy parameter for CWRC mixtures

With the dilatancy form of Eq. (27), the plastic potential $g = 0$ can be achieved through integration, and then the components of unit vector of plastic flow, denoted as $m = [m_p, m_q]^T$ at the effective stress on the loading surface (σ') can be defined as

$$m = \begin{bmatrix} m_p \\ m_q \end{bmatrix} = \frac{\partial\, g/\partial\, \sigma'}{\partial g/\partial\sigma'} \tag{28}$$

in which $\partial g/\partial\sigma'$ is evaluated applying the chain rule of differentiation

$$\frac{\partial g}{\partial\sigma'} = \frac{\partial g}{\partial p'}\frac{\partial p'}{\partial\sigma'} + \frac{\partial g}{\partial q}\frac{\partial q}{\partial\sigma'} \tag{29}$$

i.e.,

$$m_p = \frac{\partial\, g/\partial\, p'}{\sqrt{\left(\partial g/\partial p'\right)^2 + \left(\partial g/\partial q\right)^2}} = \frac{D^p}{\sqrt{D^{p2} + 1}} \tag{30}$$

and

$$m_q = \frac{\partial\, g/\partial\, q}{\sqrt{\left(\partial g/\partial p'\right)^2 + \left(\partial g/\partial q\right)^2}} = \frac{1}{\sqrt{D^{p2} + 1}} \tag{31}$$

where g is the plastic potential and m_p, m_q are the components of the plastic flow direction vectors.

5 Hardening rule

The concept of hardening in this context resembles that expressed in existing sub-loading surface models [9] and bounding surface models [32]. The hardening rule adopted in this study is assumed to take the following mathematical form as represented by Eq. (32):

$$\frac{d\left(R\overline{p'_c}\right)}{R\overline{p'_c}} = H \times \left(\frac{R\overline{p'_c}}{\overline{p'}}\right)^{-2} \times \left(\left(\overline{p'_c}\right)_{\max} - \overline{p'_c}\right) \times \frac{d\varepsilon^p_q}{\overline{p'_c}} \tag{32}$$

where

$$H = H_{\min}\left(\sigma'_3\right)^{-\beta}\exp\left(-\delta_H X_{\text{RC}}\right) \tag{33}$$

$H_{\min}$ is the minimum hardening modulus for pure granular material at $p_r = 1kPa$; β is the material parameter related to the change of confining pressure value; and δ_H presents the diminution of H with rubber content.

Figure 10 illustrates the 3D relationship between the hardening modulus, H, rubber content, X_{RC}, and the confining pressure, $\sigma_3\prime$. It is noted that when the confining pressure and the rubber content increase, the hardening modulus decreases. This is because an increase in confining pressure will result in an increase in the state parameter

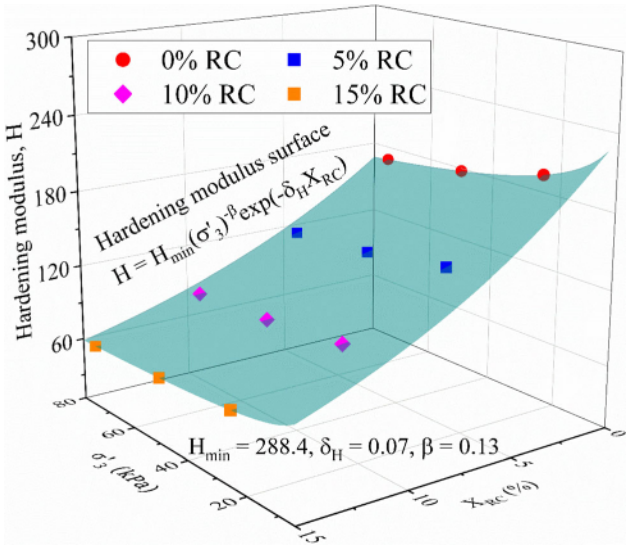

Fig. 10 Hardening modulus surface for CWRC mixtures in the $H - \sigma_3\prime - X_{RC}$ space

ψ_0,, while the increase in rubber content will cause a reduction in the stress ratio η due to the low shear strength of rubber materials, and both the increase in ψ_0 and reduction in η will reduce the material hardening modulus [17].

6 Evaluation of model parameters

The model parameters must be calibrated to accurately predict the material behaviour. Laboratory tests provide a reliable means of calibrating most model parameters, except for the hardening modulus H. The parameters in this proposed model are classified into six distinct categories: bounding surface, CS, plastic potential, elasticity, compressibility constants, and the hardening domain. The parameters defining the elastic components are elaborated in Appendix A. The parameters $M_{cs}, \Gamma_1, \Gamma_2, \lambda_1$, and λ_2 are used to define the CS surface. The values of $\Gamma_1, \Gamma_2, \lambda_1$, and λ_2 can be obtained through curve fitting, as shown in Fig. 2b. The compressibility constants e_0^* and ω_0 can be derived from Eqs. (2) and (3), respectively. The parameter N determines the degree of curvature of the bounding surface. M_{cs} and N can be determined by fitting the relationship between the plastic dilatancy and stress ratio, as shown earlier in Fig. 6. The dilatancy parameter χ can be determined from the relationship between the dilatancy and state parameter at peak deviator stress, as explained in Fig. 9. The hardening parameters H_{min}, δ_H and β can be evaluated from the relationship between the hardening modulus, confining pressure, and X_{RC} values, as illustrated earlier in Fig. 10. Table 1 summarises the model parameter values for CWRC mixtures and SFS + CW + RC mixtures.

7 Model validation and discussion

The proposed constitutive model was validated using experimental data from static triaxial tests. Figure 11a–c shows the monotonic stress–strain curves predicted by the model and the test data available for CWRC mixtures from Indraratna et al. [14] for a range of confining pressures (i.e. 25, 50 and 75 kPa) and rubber contents (i.e., 0% to 15%). The volumetric strain response of the mixtures is illustrated in Fig. 11d–f. The modified volumetric strain-based bounding surface model accurately captures the overall volumetric response and the stress–strain relationship of CWRC mixtures, and as expected, the strain hardening response and peak deviator stress increase with the confining pressures. Furthermore, as the percentage of rubber

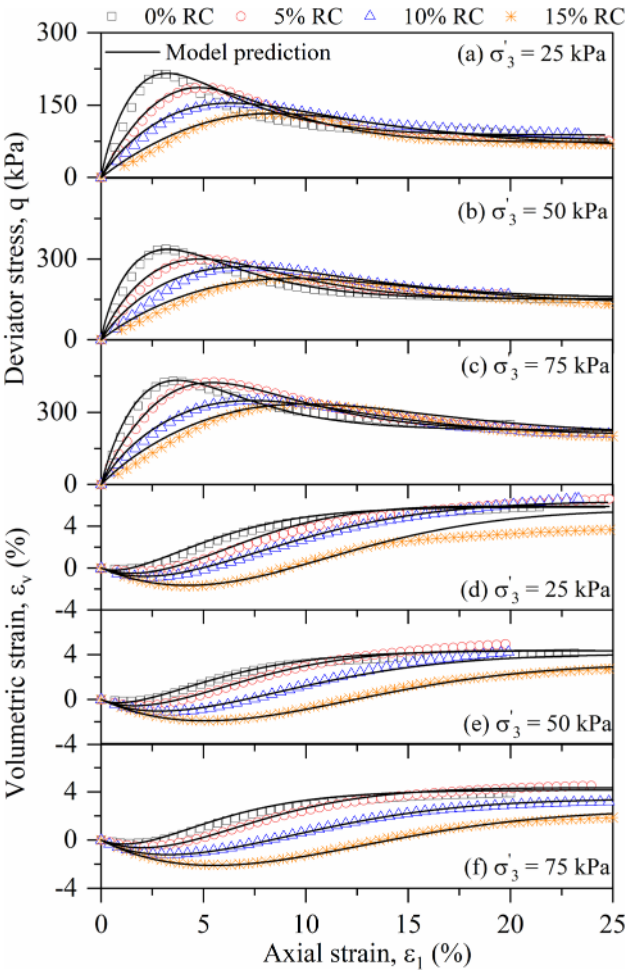

Fig. 11 Test results and model prediction for CWRC mixtures with different X_{RC} contents and confining pressure values **a–c** deviator stress, and **d–f** volumetric strain

crumbs increases, the peak deviator stress decreases, and the strain softening behaviour shifts towards strain hardening. This indicates that the specimen becomes more contractive than pure granular materials, which proves that the inclusion of rubber in the granular waste mixtures leads to a transition from a brittle to ductile behaviour. An independent set of static triaxial data for SFS + CW + RC mixtures tested by Qi et al. [26] is also used to validate the model under varying confining pressures and rubber contents. The influence of the confining pressure, $\sigma_3\prime$, on the stress–strain characteristics of SFS + CW + RC mixtures is accurately captured by the model and is similar to that observed for CWRC mixtures, as shown in Figs. 12 and 13. Nevertheless, in both Figs. 12 and 13, there is a noticeable deviation between the predicted volumetric strain response and that observed in laboratory tests. This discrepancy arises from the omission of the internal deformation of rubber in the study conducted by Qi et al. [26]. Bellotti et al. [2] indicates that the purely elastic strain typically observed in pure granular materials is generally around 0.00001. However, this may not be applicable for rubber mixed with granular materials because rubber is more elastic than hard aggregates. As a result, the introduction of rubber can lead to higher elastic strains. This could be one of the reasons for the deviations, highlighting the need to incorporate a modified void ratio or volumetric strain in the analysis.

As rubber-included granular mixtures are becoming increasingly prevalent in roads and rail infrastructure, the proposed model will be beneficial to further understand their fundamental stress–strain behaviour, as well as capturing the salient aspects of the proposed model in future numerical analysis. It has certain limitations because the bounding surface was only established for conditions where $q > 0$, and therefore, the proposed model is only applicable under compressive loading conditions.

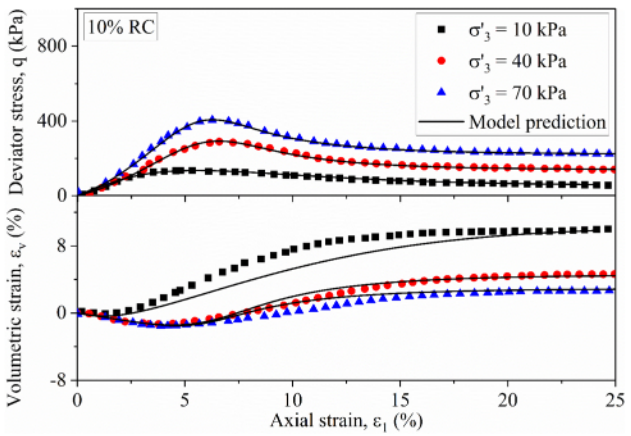

Fig. 12 Test results and model prediction for SFS63 + CW27 + RC10 (Data from Qi et al. [26])

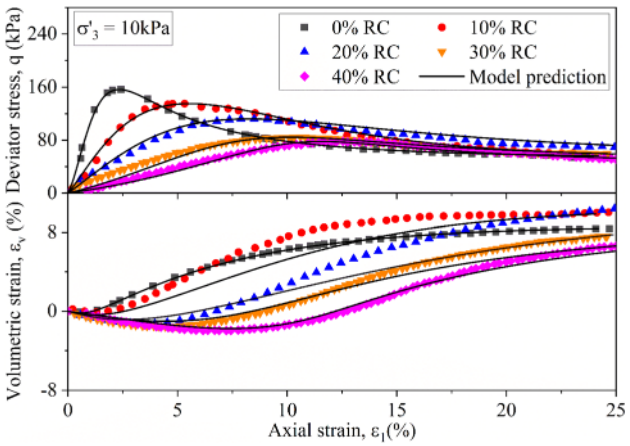

Fig. 13 Test results and model prediction for SFS + CW + RC (SFS:CW = 7:3) mixtures with different X_{RC} contents under $\sigma_3\prime$ = 10kPa (Data from Qi et al. [26])

Moreover, the compressible component in the mixtures is restricted to granulated rubber or RC; larger rubber particles such as rubber chips, may continue to deform, causing excessive volumetric strain (compression), and might not comply with the constant critical state condition. Also, despite taking extreme care with the experiments and striving for ideal conditions such as homogeneous mixing for uniform density and perfect loading conditions for the test specimens, it is not always possible to meet these conditions perfectly so there may be some disparity between the measured results and the predicted results.

8 Conclusions

In this study, a new constitutive model was developed to predict the stress–strain response of mining waste-rubber crumbs mixtures by adopting a bounding surface plasticity approach and incorporating a compressibility-dependent volumetric strain and image state of the critical state. A quantitative evaluation of the model was performed by simulating a series of test outcomes obtained from independent research studies. The main findings can be summarised as follows:

- To capture the deformation of compressible and elastic rubber crumbs in the mixture, a modified void ratio and volumetric strain were introduced in the proposed model.
- A relationship between the CSV parameters in the $e^* - lnp\prime$ plane and the rubber content, X_{RC} (%), was established and a 3D CSV surface was portrayed in the $e^* - lnp - X_{RC}$ space. This allowed for the direct incorporation of the impact of adding a compressible component like rubber on the CS of the waste granular blends. The CSVL rotates in a clockwise direction as

the RC percentages indicating the CWRC mixtures became more contractive.

- To capture the stress–strain behaviour of rubber mixed granular materials, an image state ratio-based plastic flow rule and hardening modulus (dependent on the confining pressure and the rubber content in the mixture) were adopted. The value of hardening modulus is not unique; it decreases with the increasing rubber content and the confining pressure.
- The proposed model was calibrated and validated using the laboratory data from two independent rubber-mixed waste materials, namely CWRC and SFS + CW + RC. The model predictions matched well with the test results for CWRC mixtures. However, the notable discrepancy between the model predictions and test results for SFS + CW + RC mixtures reiterates the necessity to capture the internal deformation of rubber more accurately within the granular matrix.

Appendix A: Theory of elasticity—governing equations

As per the classical soil mechanics, the incremental elastic stress–strain relationship can be expressed as:

$$d\sigma = D^e d\varepsilon^e \tag{34}$$

In the $p\prime \sim q$ plane, elasticity property matrix D^e is defined as:

$$D^e = \begin{bmatrix} B & 0 \\ 0 & 3G \end{bmatrix} \tag{35}$$

where B and G represent the tangential bulk modulus and tangential shear modulus, respectively. They can be determined by:

$$B = \frac{(1+e_0^*)p'}{\kappa} \tag{36}$$

$$G = \frac{3(1-2\mu)}{2(1+\mu)}B \tag{37}$$

where μ denotes the Poisson's ratio of the materials determined from the relationship between the radial strain and axial strain in the elastic range [34]:

$$\mu = \frac{3\varepsilon_q - 2\varepsilon_v}{6\varepsilon_q + 2\varepsilon_v} = -\frac{\varepsilon_3}{\varepsilon_1} \tag{38}$$

where ε_v andε_q presents the volumetric strain and deviator strain, respectively.

Appendix B: Initial modified void ratio

Let X denote the mass-based RC proportion and Z signify the volume-based RC proportion with respect to the CW content. X and Y are subsequently defined as follows:

$$X_{\mathrm{RC}} = \frac{m_{\mathrm{RC}}}{m_{\mathrm{CW}}} \tag{39}$$

$$Z_{\mathrm{RC}} = \frac{V_{\mathrm{RC}}}{V_{\mathrm{CW}}} \tag{40}$$

where m_{RC} and m_{CW} represent the masses of RC and CW, respectively, and V_{RC} and V_{CW} denote the volumes of RC and CW, respectively. The initial volumetric RC proportion (Z_{RC0}) is then calculated based on the assumption that there is no compression of RC prior to the beginning of shearing.

$$\begin{aligned} Z_{\mathrm{RC0}} &= \frac{V_{\mathrm{RC0}}}{V_{\mathrm{CW}}} = \frac{m_{\mathrm{RC}}/\text{density of water} \times G_{\mathrm{s,RC}}}{m_{\mathrm{CW}}/\text{density of water} \times G_{\mathrm{s,CW}}} \\ &= X_{\mathrm{RC}} \times \frac{G_{\mathrm{s,CW}}}{G_{\mathrm{s,RC}}} \end{aligned} \tag{41}$$

Tawk and Indraratna [37] stated that the traditional void ratio equation developed for incompressible aggregates, such as gravel and sand, where the volume of solids is considered constant, becomes compromised when the mixture includes a deformable and compressible component, such as rubber. In this case, the volume of solids cannot be assumed to be constant. To address this issue, they proposed a modified void ratio (e^*), defined as the ratio between the volume of voids (V_v) and the constant volume of incompressible solids (i.e., the volume of CW, V_{CW}), as presented in Eq. (42).

$$e^* = \frac{V_v}{V_{\mathrm{CW}}} = e_0^* + \varepsilon_v^*(1+\omega_0) \tag{42}$$

Before the onset of shearing, ε_v^* = 0, and the modified initial void ratio (e_0^*) can be expressed as follows:

$$\begin{aligned} e_0^* &= \frac{V_{v0}}{V_{\mathrm{CW}}} \times \frac{V_{\mathrm{CW}} + V_{\mathrm{RC0}}}{V_{\mathrm{CW}} + V_{\mathrm{RC0}}} = \frac{V_{v0}}{V_{\mathrm{CW}} + V_{\mathrm{RC0}}} \times \frac{V_{\mathrm{CW}} + V_{\mathrm{RC0}}}{V_{\mathrm{CW}}} \\ &= e_0\left(\frac{V_{\mathrm{CW}}}{V_{\mathrm{CW}}} + Z_{\mathrm{RC0}}\right) = e_0\left(1 + X_{\mathrm{RC}} \times \frac{G_{\mathrm{s,CW}}}{G_{\mathrm{s,RC}}}\right) \end{aligned} \tag{43}$$

where V_{v0} represents the volume of voids prior to the start of shearing.

Acknowledgements This research study was financially supported via UTS International Research Scholarship, c/o the Transport Research Centre (TRC), University of Technology Sydney (UTS). The financial support from Australian Research Council for the projects ARCLP200200915 and ARCDP220102862 was also acknowledged. The initial support for experimental work by the ARC ITTC-Rail is gratefully acknowledged. The occasional feedbacks from Prof Hadi

Khabbaz, Prof Cholachat Rujikiatkamjorn as well as Dr Chathuri Kulappu Arachchige, are appreciated.

Author contributions A.R. and Y.Q. wrote the main manuscript text and A.R. prepared the figures. B.I. and Y.Q. provided the funding and supervised the research. B.I. and M.R. reviewed and edited the manuscript.

Funding Open Access funding enabled and organized by CAUL and its Member Institutions.

Data availability Some or all data, models, or code that supports the findings of this study are available from the corresponding author upon reasonable request.

Declarations

Conflict of interest The authors declare no competing interests.

References

1. Been K, Jefferies MG (1985) A state parameter for sands. Géotechnique 35(2):99–112. https://doi.org/10.1680/geot.1985.35.2.99
2. Bellotti R, Ghionna V, Jamiolkowski M, Robertson PK, Peterson RW (1989) Interpretation of moduli from self-boring pressuremeter tests in sand. Géotechnique 39(2):269–292. https://doi.org/10.1680/geot.1989.39.2.269
3. Bolton MD (1986) The strength and dilatancy of sands. Géotechnique 36(1):65–78. https://doi.org/10.1680/geot.1986.36.1.65
4. Chenari RJ, Fard MK, Shafie J, Ghorbanpour A (2017) Tire shreds and tire crumbs inclusion: contrast effects on bearing capacity of sand. Electron J Geotech Eng 22(9):3649–3667
5. Chiaro G, Indraratna B, Tasalloti SMA, Rujikiatkamjorn C (2015) Optimisation of coal wash–slag blend as a structural fill. Proc Inst Civ Eng: Ground Improv 168(1):33–44. https://doi.org/10.1680/grim.13.00050
6. Dafalias YF, Popov EP (1975) A model of nonlinearly hardening materials for complex loading. Acta Mech 21(3):173–192. https://doi.org/10.1007/BF01181053
7. Duncan JM, Byrne P, Wong KS, Mabry P (1980) Strength, stress-strain and bulk modulus parameters for finite element analyses of stresses and movements in soil masses. Report No. UCB/GT/80-01, College of Engineering, Office of Research Services, University of California, Berkely, California
8. Dzaklo CK, Rujikiatkamjorn C, Indraratna B, Kelly R (2021) Cyclic behaviour of compacted black soil-coal wash matrix. Eng Geol 294:106385. https://doi.org/10.1016/j.enggeo.2021.106385
9. Hashiguchi K, Chen ZP (1998) Elastoplastic constitutive equation of soils with the subloading surface and the rotational hardening. Int J Numer Anal Methods Geomech 22:197–227
10. Heitor A, Indraratna B, Kaliboullah CI, Rujikiatkamjorn C, McIntosh GW (2016) Drained and undrained shear behavior of compacted coal wash. J Geotech Geoenviron Eng 142(5):04016006. https://doi.org/10.1061/(ASCE)GT.1943-5606.0001422
11. Hunsucker D, Sharpe GW, Rose JG, Deen RC (1987) Road base construction utilizing coal waste materials. Research Report No. UKTRP-87-15, College of Engineering, University of Kentucky, Lexington, Kentucky
12. Hunt H, Indraratna B, Qi Y (2023) Ductility and energy absorbing behaviour of coal wash–rubber crumb mixtures. Int J Rail Transp 11(4):508–528. https://doi.org/10.1080/23248378.2022.2095539
13. Indraratna B, Gasson I, Chowdhury RN (1994) Utilization of compacted coal tailings as a structural fill. Can Geotech J 31(5):614–623. https://doi.org/10.1139/t94-074
14. Indraratna B, Rujikiatkamjorn C, Tawk M, Heitor A (2019) Compaction, degradation and deformation characteristics of an energy absorbing matrix. Transp Geotech 19:74–83. https://doi.org/10.1016/j.trgeo.2019.02.002
15. Jefferies MG (1993) Nor-Sand: a simple critical state model for sand. Géotechnique 43(1):91–103. https://doi.org/10.1680/geot.1993.43.1.91
16. Jefferies M (2022) On the fundamental nature of the state parameter. Géotechnique 72(12):1082–1091. https://doi.org/10.1680/jgeot.20.P.228
17. Jefferies M, Been K (2016) Soil liquefaction: a critical state approach, 2nd edn. CRC Press, London
18. Khataei B, Nasrollahi M (2020) Optimizing the tensile strength of concrete containing coal waste considering the cost. SN Appl Sci 2:103. https://doi.org/10.1007/s42452-019-1883-4
19. Lee JH, Salgado R, Bernal A, Lovell CW (1999) Shredded tires and rubber-sand as lightweight backfill. J Geotech Geoenviron Eng 125(2):132–141. https://doi.org/10.1061/(ASCE)1090-0241(1999)125:2(132)
20. Leventhal A, De Ambrosis L (1985) Waste disposal in coal mining—a geotechnical analysis. Eng Geol 22(1):83–96. https://doi.org/10.1016/0013-7952(85)90040-7
21. Mashiri MS, Vinod JS, Sheikh MN (2016) Constitutive model for sand–tire chip mixture. Int J Geomech 16(1):04015022. https://doi.org/10.1061/(ASCE)GM.1943-5622.0000472
22. Mashiri MS, Vinod JS, Sheikh MN, Tsang HH (2015) Shear strength and dilatancy behaviour of sand–tyre chip mixtures. Soils Found 55(3):517–528. https://doi.org/10.1016/j.sandf.2015.04.004
23. Nova R, Wood D (1982) A constitutive model for soil under monotonic and cyclic loading. In: Pande GN, Zienkiewicz OC (eds) Soil mechanics-transient and cyclic loads. Wiley, New York, pp 343–373
24. Qi Y, Indraratna B, Coop MR (2019) Predicted behavior of saturated granular waste blended with rubber crumbs. Int J Geomech 19(8):04019079. https://doi.org/10.1061/(ASCE)GM.1943-5622.0001440
25. Qi Y, Indraratna B, Tawk M (2020) Use of recycled rubber elements in track stabilisation. Geo-Congress 2020:49–59
26. Qi Y, Indraratna B, Vinod JS (2018) Behavior of steel furnace slag, coal wash, and rubber crumb mixtures with special relevance to stress–dilatancy relation. J Mater Civ Eng 30(11):04018276. https://doi.org/10.1061/(ASCE)MT.1943-5533.0002459
27. Roscoe KH, Burland JB (1968) On the generalized stress-strain behavior of "wet" clay. In: Heyman J, Leckie FA (eds)

Engineering pla sticity. University of Cambridge, Cambridge, pp 535–609
28. Roscoe KH, Schofield AN (1963) Mechanical behaviour of an idealised ''wet-clay''. In: Proc 2nd Eur Conf Soil Mech and Found Eng, Wiesbaden, Germany, pp 47–54
29. Roscoe KH (1970) The influence of strains in soil mechanics. Géotechnique 20(2):129–170. https://doi.org/10.1680/geot.1970.20.2.129
30. Roscoe KH, Schofield AN, Wroth CP (1958) On the yielding of soils. Géotechnique 8(1):22–53. https://doi.org/10.1680/geot.1958.8.1.22
31. Russell AR, Khalili N (2004) A bounding surface plasticity model for sands exhibiting particle crushing. Can Geotech J 41:1179–1192. https://doi.org/10.1139/t04-065
32. Russell AR, Khalili N (2005) A unified bounding surface plasticity model for unsaturated soils. Int J Numer Anal Methods Geomech 30:181–212. https://doi.org/10.1002/nag.475
33. Stroud M (1971) The behaviour of sand at low stress levels in the simple shear apparatus. Dissertation, Univesity of Cambridge
34. Sun Y, Wichtmann T, Sumelka W, Kan ME (2020) Karlsruhe fine sand under monotonic and cyclic loads: modelling and validation. Soil Dyn Earthq Eng 133:106119. https://doi.org/10.1016/j.soildyn.2020.106119
35. Sun Y, Xiao Y, Ju W (2014) Bounding surface model for ballast with additional attention on the evolution of particle size distribution. Sci China Technol Sci 57:1352–1360. https://doi.org/10.1007/s11431-014-5575-4
36. Tasalloti SMA, Indraratna B, Rujikiatkamjorn C, Heitor A, Chiaro G (2015) A laboratory study on the shear behavior of mixtures of coal wash and steel furnace slag as potential structural fill. Geotech Test J 38(4):361–372. https://doi.org/10.1520/GTJ20140047
37. Tawk M, Indraratna B (2021) Role of rubber crumbs on the stress-strain response of a coal wash matrix. J Mater Civ Eng 33(3):04020480. https://doi.org/10.1061/(ASCE)MT.1943-5533.0003514
38. Taylor DW (1948) Fundamentals of soil mechanics. Wiley, New York
39. Wang D, Tawk M, Indraratna B, Heitor A, Rujikiatkamjorn C (2019) A mixture of coal wash and fly ash as a pavement substructure material. Transp Geotech 21:100265. https://doi.org/10.1016/j.trgeo.2019.100265
40. Wroth CP, Bassett RH (1965) A stress–strain relationship for the shearing behaviour of a sand. Géotechnique 15(1):32–56. https://doi.org/10.1680/geot.1965.15.1.32
41. Youwai S, Bergado DT (2003) Strength and deformation characteristics of shredded rubber tire sand mixtures. Can Geotech J 40:254–264. https://doi.org/10.1139/t02-104